THEORETICAL AND APPLIED MECHANICS
Volume 50 (2023) Issue 2, 185–204 DOI: https://doi.org/10.2298/TAM231017011V

ANALYTICAL AND NUMERICAL ANALYSIS OF NONISOTHERMAL COMPRESSIBLE RAREFIED GAS FLOW BETWEEN PARALLEL PLATES

Petar V. Vulićević, Snežana S. Milićev, and Nevena D. Stevanović

Abstract. When dimensions of the flow domain become small, such as in the micro-electro-mechanical systems (MEMS) and nano-electro-mechanical systems (NEMS), rarefaction effects become more prominent. Flows that we consider are in the continuum and rarefied gas flow regimes. We provide analytical solutions for compressible nonisothermal flows between parallel plates, with different temperatures. Comparison of results between our analytical solutions and commercial CFD code Ansys Fluent is performed. We analyze four cases with constant and variable transport coefficients in both continuum and rarefied gas flow regimes. The analysis reveals that very good agreement is present in the continuum flow regime, as well as in the slip flow regime. This outcome not only validates the present study but also opens up opportunities to investigate cases where analytical solutions are unobtainable.

1. Introduction

The characteristics of fluid flow through small domains, at micro or nano scales, have been extensively studied. Devices operating under these conditions are known as micro-electro-mechanical systems (MEMS) and nano-electro-mechanical systems (NEMS). This topic has been extensively explored in many books that provide comprehensive reviews of analytical solutions, experimental investigations, and numerical methods applied to these problems [1, 2]. Furthermore, many review papers have delved into this subject [3, 4, 5].

In the domain of rarefied gas flow regimes, a variety of Computational Fluid Dynamics (CFD) codes are available for their modeling. In particular, Scanlon et al. [6] coded a new module named dsmcFoam for open CFD code OpenFOAM, based on Direct simulation Monte Carlo (DSMC). They modeled both transient and steady flows of arbitrary 2D and 3D geometries.

2020 *Mathematics Subject Classification:* 76N15; 76P99.
Key words and phrases: analytical solutions, perturbation methods, rarefied gas flow, slip flow, continuum flow, nonisothermal, compressible.

In the slip flow regime, numerical solutions based on continuum equations, supplied with velocity slip and temperature jump boundary conditions, have been proven to be highly effective. Some commercial CFD codes incorporate this to solve problems in the slip flow regime. Spiga and Vocale [7] used COMSOL Multiphysics to simulate flow in the slip regime with constant heat flux for rectangular and tubular cross sections. Pitakarnnop et al. [8] used Ansys Fluent to model isothermal flows in the slip flow regime, also for both rectangular and tubular flow domains. Ansys Fluent has also been used to model nonisothermal flows with streamwise temperature gradient (creep flow) [9].

In this paper, we derive analytical solutions for nonisothermal problems in both rarefied and continuum flow domains. The nonisothermal effects are driven by temperature difference between the walls. We also examine these problems using Ansys Fluent and compare the results to the corresponding analytical solutions. This analysis enables us to explore the potential and reliability of Ansys Fluent for expanding its applicability to rarefied gas flow domains, which is especially valuable for cases where obtaining analytical solutions proves challenging.

We begin by introducing the problem, including the governing equations, boundary conditions, and underlying assumptions. Subsequently, analytical solutions are provided, covering both the continuum and rarefied gas flow regimes. Following this, setup of numerical analysis is presented. Finally, we conclude with an in-depth analysis of the results and the conclusions drawn from this study.

1.1. Problem description. We will consider nonisothermal and compressible gas flows between parallel plates, for continuum and rarefied regimes (Figure 1). It is nonisothermal, since the top and bottom walls are at different temperatures, while it is compressible since we are studying flows of gases. This is pressure driven flow where inlet pressure is p_i and outlet pressure is p_o. The components of velocity are represented in Cartesian coordinate system where u represents streamwise component and v crosswise component. In our case we consider only channels whose length l is significantly larger than their height h.

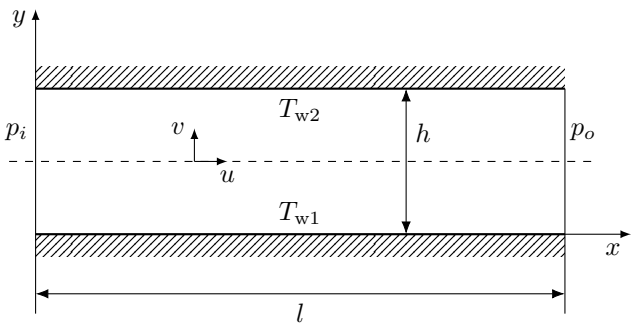

FIGURE 1. Flow domain

1.2. Governing equations. To describe this problem mathematically, laws of conservation of mass, momentum, and energy, as well as the equation of state, and appropriate boundary conditions will be implemented. Since the flows considered in this paper are in the continuum and slip flow regimes, i.e. $\mathrm{Kn} < 0.1$, it is sufficient to use equations and boundary conditions of order of Knudsen number, $\mathcal{O}(\mathrm{Kn})$ [2].

1.2.1. *Governing equations in dimensional form.* For steady two-dimensional flows of viscous fluid, equations of conservation of mass, momentum, and energy take the following form:

$$\frac{\partial(\tilde{\rho}\tilde{u})}{\partial\tilde{x}} + \frac{\partial(\tilde{\rho}\tilde{v})}{\partial\tilde{y}} = 0 \tag{1.1}$$

$$\tilde{\rho}\Big(\tilde{u}\frac{\partial\tilde{u}}{\partial\tilde{x}} + \tilde{v}\frac{\partial\tilde{u}}{\partial\tilde{y}}\Big) = -\frac{\partial\tilde{p}}{\partial\tilde{x}} + \frac{\partial}{\partial\tilde{x}}\Big[2\tilde{\mu}\frac{\partial\tilde{u}}{\partial\tilde{x}} - \frac{2}{3}\tilde{\mu}\Big(\frac{\partial\tilde{u}}{\partial\tilde{x}} + \frac{\partial\tilde{v}}{\partial\tilde{y}}\Big)\Big] + \frac{\partial}{\partial\tilde{y}}\Big[\tilde{\mu}\Big(\frac{\partial\tilde{u}}{\partial\tilde{y}} + \frac{\partial\tilde{v}}{\partial\tilde{x}}\Big)\Big] \tag{1.2}$$

$$\tilde{\rho}\Big(\tilde{u}\frac{\partial\tilde{v}}{\partial\tilde{x}} + \tilde{v}\frac{\partial\tilde{v}}{\partial\tilde{y}}\Big) = -\frac{\partial\tilde{p}}{\partial\tilde{y}} + \frac{\partial}{\partial\tilde{y}}\Big[2\tilde{\mu}\frac{\partial\tilde{v}}{\partial\tilde{y}} - \frac{2}{3}\tilde{\mu}\Big(\frac{\partial\tilde{u}}{\partial\tilde{x}} + \frac{\partial\tilde{v}}{\partial\tilde{y}}\Big)\Big] + \frac{\partial}{\partial\tilde{x}}\Big[\tilde{\mu}\Big(\frac{\partial\tilde{u}}{\partial\tilde{y}} + \frac{\partial\tilde{v}}{\partial\tilde{x}}\Big)\Big] \tag{1.3}$$

$$\begin{aligned}\tilde{\rho}c_p\Big(\tilde{u}\frac{\partial\tilde{T}}{\partial\tilde{x}} + \tilde{v}\frac{\partial\tilde{T}}{\partial\tilde{y}}\Big) &= \tilde{u}\frac{\partial\tilde{p}}{\partial\tilde{x}} + \tilde{v}\frac{\partial\tilde{p}}{\partial\tilde{y}} + \frac{\partial}{\partial\tilde{x}}\Big(\tilde{k}\frac{\partial\tilde{T}}{\partial\tilde{x}}\Big) + \frac{\partial}{\partial\tilde{y}}\Big(\tilde{k}\frac{\partial\tilde{T}}{\partial\tilde{y}}\Big)\\ &\quad + \tilde{\mu}\Big[2\Big(\frac{\partial\tilde{u}}{\partial\tilde{x}}\Big)^2 + 2\Big(\frac{\partial\tilde{v}}{\partial\tilde{y}}\Big)^2 + \Big(\frac{\partial\tilde{u}}{\partial\tilde{y}} + \frac{\partial\tilde{v}}{\partial\tilde{x}}\Big)^2 - \frac{2}{3}\Big(\frac{\partial\tilde{u}}{\partial\tilde{x}} + \frac{\partial\tilde{v}}{\partial\tilde{y}}\Big)^2\Big]\end{aligned} \tag{1.4}$$

$$\tilde{p} = \tilde{\rho}\tilde{R}\tilde{T} \tag{1.5}$$

Here, and in all subsequent sections, dimensional quantities are denoted with tilde sign over ($\sim$), while nondimensional quantities are not.

1.2.2. *Nondimensionalization of equations and assumptions.* All equations will be nondimensionalized with their reference values. In this paper, the following values are used as reference values: channel length $\tilde{l}$ for streamwise coordinate $\tilde{x}$, channel height $\tilde{h}$ for crosswise coordinate $\tilde{y}$, the average value of the velocity at outlet cross section $\tilde{u}_{\mathrm{r}}$ for velocity, outlet pressure $\tilde{p}_o$ for pressure, average temperature between channel walls $\tilde{T}_r = (\tilde{T}_{\mathrm{w}2} + \tilde{T}_{\mathrm{w}1})/2$ for temperature.

Reference values of transport coefficients, dynamic viscosity $\tilde{\mu}_{\mathrm{r}}$, and thermal conductivity $\tilde{k}_{\mathrm{r}}$, were calculated with reference temperature, $\tilde{T}_r$. Nondimensional values of transport coefficients were defined according to the hard sphere model [10] with viscosity-temperature index a as:

$$\mu = \frac{\tilde{\mu}}{\tilde{\mu}_{\mathrm{r}}} = T^a, \quad k = \frac{\tilde{k}}{\tilde{k}_{\mathrm{r}}} = T^a \tag{1.6}$$

Reference Mach, Reynolds and Prandtl numbers, that appear in nondimensional form of equations (1.1)–(1.5), are defined in the following way:

$$\mathrm{Ma}_{\mathrm{r}} = \frac{\tilde{u}_{\mathrm{r}}}{\sqrt{\kappa\tilde{R}\tilde{T}_r}}, \quad \mathrm{Re}_{\mathrm{r}} = \frac{\tilde{u}_{\mathrm{r}}\tilde{h}_{\mathrm{r}}\tilde{p}_o}{\tilde{\mu}_{\mathrm{r}}\tilde{R}\tilde{T}_r}, \quad \mathrm{Pr}_{\mathrm{r}} = \mathrm{Pr} = \frac{\tilde{c}_p\tilde{\mu}}{\tilde{k}}$$

where $\tilde{c}_p$ is specific heat at constant pressure.

Now system of governing equations (1.1)–(1.5), has the following nondimensional form:

$$\frac{\partial(\rho u)}{\partial x}+\frac{\tilde{l}}{\tilde{h}}\frac{\partial(\rho v)}{\partial y}=0 \tag{1.7}$$

$$\begin{aligned}\kappa \mathrm{Ma}_{\mathrm{r}}^{2}\rho\Big(\frac{\tilde{h}}{\tilde{l}}u\frac{\partial u}{\partial x}+v\frac{\partial u}{\partial y}\Big)=&-\frac{\tilde{h}}{\tilde{l}}\frac{\partial p}{\partial x}+\frac{\kappa \mathrm{Ma}_{\mathrm{r}}^{2}}{\mathrm{Re}_{\mathrm{r}}}\frac{\tilde{h}}{\tilde{l}}\Big[\frac{\tilde{h}}{\tilde{l}}2\mu\frac{\partial u}{\partial x}-\frac{2}{3}\mu\Big(\frac{\tilde{h}}{\tilde{l}}\frac{\partial u}{\partial x}+\frac{\partial v}{\partial y}\Big)\Big]\\&+\frac{\kappa \mathrm{Ma}_{\mathrm{r}}^{2}}{\mathrm{Re}_{\mathrm{r}}}\frac{\partial}{\partial y}\Big[\mu\Big(\frac{\partial u}{\partial y}+\frac{\tilde{h}}{\tilde{l}}\frac{\partial v}{\partial x}\Big)\Big]\end{aligned} \tag{1.8}$$

$$\begin{aligned}\kappa \mathrm{Ma}_{\mathrm{r}}^{2}\rho\Big(\frac{\tilde{h}}{\tilde{l}}u\frac{\partial v}{\partial x}+v\frac{\partial v}{\partial y}\Big)=&-\frac{\partial p}{\partial y}+\frac{\kappa \mathrm{Ma}_{\mathrm{r}}^{2}}{\mathrm{Re}_{\mathrm{r}}}\Big[2\mu\frac{\partial v}{\partial y}-\frac{2}{3}\mu\Big(\frac{\tilde{h}}{\tilde{l}}\frac{\partial u}{\partial x}+\frac{\partial v}{\partial y}\Big)\Big]\\&+\frac{\kappa \mathrm{Ma}_{\mathrm{r}}^{2}}{\mathrm{Re}_{\mathrm{r}}}\frac{\partial}{\partial x}\Big[\mu\Big(\frac{\partial u}{\partial y}+\frac{\tilde{h}}{\tilde{l}}\frac{\partial v}{\partial x}\Big)\Big]\end{aligned} \tag{1.9}$$

$$\begin{aligned}\mathrm{Re}_{\mathrm{r}}\mathrm{Pr}\rho\Big(\frac{\tilde{h}}{\tilde{l}}u\frac{\partial T}{\partial x}+v\frac{\partial T}{\partial y}\Big)=&\,\mathrm{Re}_{\mathrm{r}}\mathrm{Pr}\frac{(\kappa-1)}{\kappa}\Big(\frac{\tilde{h}}{\tilde{l}}u\frac{\partial p}{\partial x}+v\frac{\partial p}{\partial y}\Big)+\frac{\tilde{h}^{2}}{\tilde{l}^{2}}\frac{\partial}{\partial x}\Big(k\frac{\partial T}{\partial x}\Big)\\&+\frac{\partial}{\partial y}\Big(k\frac{\partial T}{\partial y}\Big)+(\kappa-1)\mathrm{Ma}_{\mathrm{r}}^{2}\mathrm{Pr}\Big[\frac{2\tilde{h}^{2}}{\tilde{l}^{2}}\Big(\frac{\partial u}{\partial x}\Big)^{2}\\&+2\Big(\frac{\partial v}{\partial y}\Big)^{2}+\Big(\frac{\partial u}{\partial y}+\frac{\tilde{h}}{\tilde{l}}\frac{\partial v}{\partial x}\Big)^{2}-\frac{2}{3}\Big(\frac{\tilde{h}}{\tilde{l}}\frac{\partial u}{\partial x}+\frac{\partial v}{\partial y}\Big)^{2}\Big]\end{aligned} \tag{1.10}$$

$$p=\rho T \tag{1.11}$$

In order to simplify this system of governing equations, the following assumptions and relations between the parameters are introduced.

In this paper, we are considering channels whose height is significantly smaller than their length. Thus we can define small parameter $\varepsilon \ll 1$, as the ratio of channel height to length:

$$\varepsilon=\tilde{h}/\tilde{l} \tag{1.12}$$

We will only consider channels with parallel plates, where the crosswise velocity projection, $\tilde{v}$, is much smaller than the streamwise component. Thus, the following can be assumed [11, 12]:

$$\tilde{v}=\varepsilon\tilde{V} \tag{1.13}$$

where $\tilde{V}=\mathcal{O}(1)$. This ensures that both terms in the continuity equation are of the same order. Since fluid flow is strictly subsonic, the following can be supposed:

$$\kappa \mathrm{Ma}_{\mathrm{r}}^{2}=\beta\varepsilon^{\mathrm{m}},\quad \frac{\kappa \mathrm{Ma}_{\mathrm{r}}^{2}}{\mathrm{Re}_{\mathrm{r}}}=\gamma\varepsilon \tag{1.14}$$

where $\beta=\mathcal{O}(1),\gamma=\mathcal{O}(1)$, and exponent m has positive value, $\mathrm{m}>0$. Moreover, from assumptions (1.14), for small Reynolds numbers, parameter m is $m>1$.

Now by applying assumptions (1.12)–(1.14) to the system of governing equations (1.7)–(1.11), and by neglecting terms of order $\mathcal{O}(\varepsilon^m)$ and smaller, we obtain the system of equations for small Reynolds numbers:

$$\frac{\partial(\rho u)}{\partial x} + \frac{\partial(\rho V)}{\partial y} = 0 \tag{1.15}$$

$$\frac{\partial p}{\partial x} = \gamma \frac{\partial}{\partial y}\Big(\mu \frac{\partial u}{\partial y}\Big) \tag{1.16}$$

$$\frac{\partial p}{\partial y} = 0 \tag{1.17}$$

$$\frac{\partial}{\partial y}\Big(k \frac{\partial T}{\partial y}\Big) = 0 \tag{1.18}$$

$$p = \rho T \tag{1.19}$$

2. Analytical solutions

From the system of governing equations and their boundary conditions, solutions for both continuum and slip flow regimeswill be presented. We will start with the flow in the continuum regime, first introducing flow with constant, and then with variable transport coefficients. Afterward, the same procedure will be repeated for the flow in the slip regime. In all cases, expressions for mass flow rate, pressure, velocity and temperature distributions will be given.

2.1. Continuum gas flow. In the continuum flow regime, we apply no velocity slip and no temperature jump boundary conditions. This ensures that gas velocity and temperature match the velocity and the temperature of the wall. In the case of fixed walls, the boundary conditions are as follows:

$$\begin{aligned} u|_{y=0} &= 0, \quad V|_{y=0} = 0 \\ u|_{y=1} &= 0, \quad V|_{y=1} = 0 \end{aligned} \tag{2.1}$$

$$\begin{aligned} T|_{y=0} &= T_{\mathrm{w1}} \\ T|_{y=1} &= T_{\mathrm{w2}} \end{aligned} \tag{2.2}$$

2.1.1. *Flow in the continuum regime with constant transport coefficients.* In this subsection, we neglect the dependence of dynamic viscosity and thermal conductivity on temperature, so viscosity-temperature index $a = 0$. Consequently, relations (1.6) simplify to $\mu = 1$ and $k = 1$. We begin by solving energy equation (1.18) with appropriate temperature boundary conditions (2.2), from which we obtain temperature distribution:

$$T = (T_{\mathrm{w2}} - T_{\mathrm{w1}})y + T_{\mathrm{w1}} \tag{2.3}$$

Next, from the equation of conservation of momentum (1.16) and the application of no-slip boundary conditions (2.1), velocity distribution is obtained:

$$u = \frac{p_0'}{2\gamma}(y^2 - y) \tag{2.4}$$

Here, the prime symbol ($'$) denotes a derivative along the streamwise coordinate x. From the integral form of the continuity equation:

$$\int_0^1 \frac{pu}{T}\mathrm{d}y = \dot{m}$$

a differential equation for pressure distribution is obtained. By integrating this equation, from an arbitrary $(x,\ p)$ cross section to the outlet $(x = 1,\ p_o = 1)$ cross section, pressure distribution along the channel is obtained:

$$p = \sqrt{1 - \frac{\dot{m}}{C_I}(1 - x)} \tag{2.5}$$

Before we define constant C_I, in order to simplify our notation, the following convention for denoting constants will be adopted: the difference $T^n_{\mathrm{w}2} - T^n_{\mathrm{w}1}$ will be denoted as ΔT_n, while the addition $T^n_{\mathrm{w}2} + T^n_{\mathrm{w}1}$ will be denoted as ΔT_{n+}. Now, C_I is defined in the following way:

$$C_I = -\frac{\Delta T_{1+}}{8\gamma \Delta T_1^2} + \frac{T_{\mathrm{w}1}T_{\mathrm{w}2}}{4\gamma \Delta T_1^3}\ln\frac{T_{\mathrm{w}2}}{T_{\mathrm{w}1}}.$$

When we evaluate equation (2.5) at the inlet cross section, i.e. $x = 0$, we obtain a correlation between the mass flow rate and the pressure ratio between channel inlet and outlet pressures, $\Pi = \frac{\tilde{p}_i}{\tilde{p}_o} = p_i$.

$$\dot{m} = C_I(1 - \Pi^2) \tag{2.6}$$

There are two ways we can approach this problem. If the pressure ratio at the channel inlet and outlet is given, we can calculate the mass flow rate, and than determine other quantities of interest. The other possibility is if initial mass flow rate is known. Thus, pressure ratio at channel inlet and outlet can be obtained, and other relevant quantities can be obtained in a similar manner.

2.1.2. *Flow in the continuum regime with variable transport coefficients.* The flow considered in this section is also in the continuum regime, but this time with variable transport coefficients. Here, the dependence of transport coefficients on temperature is defined by (1.6).

The procedure for obtaining analytical solutions remains the same as for the constant transport coefficients. The analytical solution to this problem is given below:

$$T = (\Delta T_{a+1}y + T^{a+1}_{\mathrm{w}1})^{\frac{1}{a+1}} \tag{2.7}$$

$$u = \frac{(a+1)p_0'}{\gamma(a+2)\Delta T^2_{a+1}}\Big(T^{a+2} - \frac{\Delta T_{a+2}}{\Delta T_1}T + \frac{\Delta T_{a+1}T_{\mathrm{w}1}T_{\mathrm{w}2}}{\Delta T_1}\Big) \tag{2.8}$$

$$p = \sqrt{1 - \frac{2}{C_{II}}\dot{m}(1 - x)} \tag{2.9}$$

$$\dot{m} = \frac{C_{II}}{2}(1 - \Pi^2) \tag{2.10}$$

where constant C_{II} is:

$$C_{II} = -\frac{a+1}{\gamma(a+2)\Delta T_{a+1}^2}\left(\frac{T_{\mathrm{w}1}T_{\mathrm{w}2}\Delta T_a}{a\Delta T_1} + \frac{\Delta T_{a+1+}}{2}\right)$$

2.2. Rarefied gas flow. In the case of rarefied gas flow, the continuum hypothesis is violated, and the level of rarefaction will be determined by the Knudsen number. We define a reference Knudsen number as:

$$\mathrm{Kn}_{\mathrm{r}} = \frac{\tilde{\lambda}_r}{\tilde{h}_r}$$

where $\tilde{\lambda}_r = \tilde{\mu}_r/\tilde{p}_o\sqrt{0.5\pi\tilde{R}\tilde{T}_r}$ is mean free path.

In this paper, we focus on the slip flow regime, where Knudsen numbers range from 0.01 to 0.1. To maintain the Knudsen number within this regime across the entire channel, we defined reference Knudsen number at the outlet cross section. This choice has been made due to the fact that the pressure decreases along the streamwise direction, and has the lowest value at the outlet cross-section. This ensures that the value of the Knudsen number is highest at the outlet cross section, and thus that the flow in the entire channel stays within the slip regime.

In the slip flow regime, equations (1.15)–(1.19) can still be used, but with suitable boundary conditions. Since velocity slip and temperature jump are present, we will use Maxwell [14] and Smoluchowski [15] boundary conditions. In our case, these boundary conditions take the following nondimensional form:

$$u|_{y=0} = \alpha_v \mathrm{Kn}_{\mathrm{r}} \frac{T^{(0.5+a)}}{p}\frac{\partial u}{\partial y}\Big|_{y=0}, \quad V|_{y=0} = 0$$

$$u|_{y=1} = \alpha_v \mathrm{Kn}_{\mathrm{r}} \frac{T^{(0.5+a)}}{p}\frac{\partial u}{\partial y}\Big|_{y=1}, \quad V|_{y=1} = 0$$

$$T|_{y=0} = 1 + \Theta + \alpha_T \mathrm{Kn}_{\mathrm{r}} \frac{T^{(0.5+a)}}{p}\frac{\partial T}{\partial y}\Big|_{y=0}$$

$$T|_{y=1} = 1 - \Theta - \alpha_T \mathrm{Kn}_{\mathrm{r}} \frac{T^{(0.5+a)}}{p}\frac{\partial T}{\partial y}\Big|_{y=1}$$

where parameter Θ is defined in the following way:

$$\Theta = -\frac{\Delta T_1}{2} = \frac{\tilde{T}_{\mathrm{w}1} - \tilde{T}_{\mathrm{w}2}}{\tilde{T}_{\mathrm{w}1} + \tilde{T}_{\mathrm{w}2}}$$

Parameters α_v and α_T are defined as:

$$\alpha_v = \frac{(2-\sigma_v)}{\sigma_v}, \quad \alpha_T = \frac{(2-\sigma_T)}{\sigma_T}\frac{2\kappa}{\kappa+1}\frac{1}{Pr}$$

where σ_v and σ_T are momentum and temperature transport coefficients (see refs. [11, 12]). Their values range from 0 for specular reflection to 1 for diffuse reflection.

Exact analytical solutions in the slip regime are impossible to obtain, thus, they are obtained with the perturbation method. Here pressure, velocity, and temperature are assumed as perturbation expansion:

$$\varphi = \varphi_0 + \mathrm{Kn}_{\mathrm{r}}\varphi_1 + \mathcal{O}(\mathrm{Kn}_{\mathrm{r}}{}^2), \tag{2.11}$$

where φ is solution, while φ_0 and φ_1 are the first and the second approximation, respectively. The first approximation, φ_0, corresponds to the exact solution in the continuum flow regime, while all the subsequent approximations correspond to the corrections for the slip flow regime. In this paper, we will use only the first two approximations.

By substituting pressure, velocity and temperature as perturbation expansions (2.11), into the system of equations and boundary conditions, and by extracting terms of $\mathcal{O}(1)$ and $\mathcal{O}(\mathrm{Kn_r})$, we obtain two systems of equations. The second system of equations, where all terms of $\mathcal{O}(\mathrm{Kn_r})$ are extracted, corresponds to the system of equations for the second perturbation:

$$\frac{\partial}{\partial x}\Big(\frac{p_0u_1}{T_0}-\frac{p_0T_1u_0}{T_0^2}+\frac{p_1u_0}{T_0}\Big)+\frac{\partial}{\partial y}\Big(\frac{p_0V_1}{T_0}-\frac{p_0T_1V_0}{T_0^2}+\frac{p_1V_0}{T_0}\Big)=0 \tag{2.12}$$

$$p_0'=\frac{\partial}{\partial y}\Big(T_0^a\frac{\partial u_1}{\partial y}+aT_1T_0^{a-1}\frac{\partial u_0}{\partial y}\Big) \tag{2.13}$$

$$\frac{\partial}{\partial y}\Big(T_0^a\frac{\partial T_1}{\partial y}+aT_1T_0^{a-1}\frac{\partial T_0}{\partial y}\Big)=0 \tag{2.14}$$

$$\begin{aligned} u_1|_{y=0}&=\frac{\alpha_v T_{\mathrm{w1}}^{a+0.5}}{p_0}\frac{\partial u_0}{\partial y}\Big|_{y=0}, \qquad V_1|_{y=0}=0\\ u_1|_{y=1}&=\frac{-\alpha_v T_{\mathrm{w2}}^{a+0.5}}{p_0}\frac{\partial u_0}{\partial y}\Big|_{y=1}, \quad V_1|_{y=1}=0 \end{aligned} \tag{2.15}$$

$$\begin{aligned} T_1|_{y=0}&=\frac{\alpha_T T_{\mathrm{w1}}^{a+0.5}}{p_0}\frac{\partial T_0}{\partial y}\Big|_{y=0}\\ T_1|_{y=1}&=\frac{-\alpha_T T_{\mathrm{w2}}^{a+0.5}}{p_0}\frac{\partial T_0}{\partial y}\Big|_{y=1} \end{aligned} \tag{2.16}$$

This system of equations and boundary conditions will be used for both cases with constant and variable transport coefficients.

2.2.1. *Flow in the slip regime with constant transport coefficients.* As was the case in subsection 2.1.1, dependence of dynamic viscosity and thermal conductivity on temperature is neglected, so viscosity-temperature index $a = 0$. The solution for the first approximation is the same as the solution obtained for the continuum regime (2.3)–(2.6). The solution for the second approximation is obtained from the modified system of equations (2.12)–(2.14) and boundary conditions (2.15),(2.16) obtained for $a = 0$:

$$\frac{\partial}{\partial x}\Big(\frac{p_0u_1}{T_0}-\frac{p_0T_1u_0}{T_0^2}+\frac{p_1u_0}{T_0}\Big)+\frac{\partial}{\partial y}\Big(\frac{p_0V_1}{T_0}-\frac{p_0T_1V_0}{T_0^2}+\frac{p_1V_0}{T_0}\Big)=0 \tag{2.17}$$

$$\frac{\partial}{\partial x}\underbrace{\int_0^1\Big(\frac{p_0u_1}{T_0}-\frac{p_0T_1u_0}{T_0^2}+\frac{p_1u_0}{T_0}\Big)\mathrm{d}y}_{\dot{m}_1}=0 \tag{2.18}$$

$$p_1'=\gamma\frac{\partial^2u_1}{\partial y^2} \tag{2.19}$$

$$\frac{\partial^2 T_1}{\partial y^2} = 0 \tag{2.20}$$

$$\begin{aligned} u_1|_{y=0} &= \frac{\alpha_v T_{\mathrm{w1}}^{0.5}}{p_0}\frac{\partial u_0}{\partial y}\Big|_{y=0}, \qquad V_1|_{y=0} = 0 \\ u_1|_{y=1} &= \frac{-\alpha_v T_{\mathrm{w2}}^{0.5}}{p_0}\frac{\partial u_0}{\partial y}\Big|_{y=1}, \qquad V_1|_{y=1} = 0 \end{aligned} \tag{2.21}$$

$$T_1|_{y=0} = \frac{\alpha_T T_{\mathrm{w1}}^{0.5}}{p_0}\frac{\partial T_0}{\partial y}\Big|_{y=0} \quad T_1|_{y=1} = \frac{-\alpha_T T_{\mathrm{w2}}^{0.5}}{p_0}\frac{\partial T_0}{\partial y}\Big|_{y=1} \tag{2.22}$$

Here, continuity equation (2.18) is an integral form of equation (2.12). This system of equations and boundary conditions will be solved in the same way as in the continuum regime. The final solution, which comprises both approximations, according to (2.11), follows:

$$T = T_0 + \mathrm{Kn_r} T_1 = \Delta T_1 y + T_{\mathrm{w1}} + \mathrm{Kn_r}\frac{\alpha_T \Delta T_1}{p_0}\big(- \Delta T_{0.5+} y + \sqrt{T_{\mathrm{w1}}}\big) \tag{2.23}$$

$$\begin{aligned} u = u_0 + \mathrm{Kn_r} u_1 = {} & \frac{p_0{}'}{2\gamma}(y^2 - y) \\ & + \mathrm{Kn_r}\Big[\frac{p_1'}{2\gamma}y^2 - \Big(\frac{\alpha_v}{p_0}\frac{p_0'}{2\gamma}\Delta T_{0.5} + \frac{p_1'}{2\gamma}\Big)y - \frac{\alpha_v\sqrt{T_{\mathrm{w1}}}}{2\gamma}\frac{p_0'}{p_0}\Big] \end{aligned} \tag{2.24}$$

$$p = p_0 + \mathrm{Kn_r} p_1 = p_0 + \mathrm{Kn_r}\frac{C_{III}}{2C_I}\Big(\frac{\Pi - 1}{p_0}(1 - x) + \frac{1}{p_0} - 1\Big) \tag{2.25}$$

$$\dot{m} = C_I(1 - \Pi^2) + \mathrm{Kn_r}(1 - \Pi)C_{III} \tag{2.26}$$

where p_0 is solution in the continuum regime with constant transport coefficients (2.5). Constant C_{III} is defined as:

$$\begin{aligned} C_{III} = {} & -\frac{\alpha_v \Delta T_{0.5}}{2\gamma \Delta T_1^2}\Big(\sqrt{T_{\mathrm{w1}}T_{\mathrm{w2}}}\ln\frac{T_{\mathrm{w2}}}{T_{\mathrm{w1}}} + \Delta T_1\Big) \\ & + \frac{\alpha_T \Delta T_{0.5+}}{2\gamma \Delta T_1^3}\Big[\sqrt{T_{\mathrm{w1}}T_{\mathrm{w2}}}\Big(\Delta T_{1+}\ln\frac{T_{\mathrm{w2}}}{T_{\mathrm{w1}}} - 2\Delta T_1\Big) + 4\gamma \Delta T_1^3 C_I\Big] \end{aligned}$$

The relation between ratios of mass flow rates in the slip (2.26) and continuum (2.6) flow regimes, and pressure ratios Π, for constant transport coefficients is:

$$\frac{\dot{m}}{\dot{m}_0} = 1 + \mathrm{Kn_r}\frac{C_{III}}{C_I(1 + \Pi)} \tag{2.27}$$

2.2.2. *Flow in the slip regime with variable transport coefficients.* In this case, the dependence of dynamic viscosity and thermal conductivity on temperature is defined according to relations (1.6). As was the case in the previous subsection, the solution for the first approximation is the same as the exact solution in the continuum regime (2.7)–(2.10). In order to obtain a solution for the second approximation, the system of equations (2.12)–(2.14) and boundary conditions (2.15), (2.16) has to be solved. This time, it is convenient to transform y coordinate with T_0 from equation (2.3). Now, this system of equations and boundary conditions takes the following form:

$$\frac{\partial}{\partial x}\underbrace{\int_{T_{w1}}^{T_{w2}}(p_0u_1T_0^{a-1}-p_0T_1u_0T_0^{a-2}+p_1u_0T_0^{a-1})\mathrm{d}T_0}_{\dot m_1}=0 \tag{2.28}$$

$$p_1'=\frac{\gamma\Delta T_{a+1}^2}{(a+1)^2T_0^a}\frac{\partial}{\partial T_0}\Big(\frac{\partial u_1}{\partial T_0}+a\frac{T_1}{T_0}\frac{\partial u_0}{\partial T_0}\Big) \tag{2.29}$$

$$\frac{\partial}{\partial T_0}\Big(a\frac{T_1}{T_0}+\frac{\partial T_1}{\partial T_0}\Big)=0 \tag{2.30}$$

$$\begin{aligned} u_1|_{y=0}&=\frac{\alpha_vT_{w1}^{0.5}p_0'}{\gamma(a+2)\Delta T_1\Delta T_{a+1}p_0}((a+2)T_{w1}^{a+1}\Delta T_1-\Delta T_{a+2}),\quad V_1|_{y=0}=0\\ u_1|_{y=1}&=\frac{-\alpha_vT_{w2}^{0.5}p_0'}{\gamma(a+2)\Delta T_1\Delta T_{a+1}p_0}((a+2)T_{w2}^{a+1}\Delta T_1-\Delta T_{a+2}),\quad V_1|_{y=1}=0\end{aligned} \tag{2.31}$$

$$\begin{aligned} T_1|_{y=0}&=\frac{\alpha_TT_{w1}^{0.5}\Delta T_{a+1}}{(a+1)p_0}\\ T_1|_{y=1}&=\frac{-\alpha_TT_{w2}^{0.5}\Delta T_{a+1}}{(a+1)p_0}\end{aligned} \tag{2.32}$$

Here, continuity equation (2.12) is written only in its integral form (2.28). The second approximations for pressure, velocity and temperature are obtained for system (2.28)–(2.32) in the same way as in the first approximation (continuum). The final solution is obtained when both approximations are substituted into the perturbation expansion (2.11), and it takes the following form:

$$T=T_0+\mathrm{Kn_r}T_1=T_0+\mathrm{Kn_r}\Big[-\frac{\alpha_T\Delta T_{a+0.5+}}{(a+1)p_0}T_0+\frac{\alpha_TT_{w1}^{a+0.5}T_{w2}^{a+0.5}\Delta T_{0.5+}}{(a+1)p_0}T_0^{-a}\Big] \tag{2.33}$$

$$\begin{aligned} u=u_0+\mathrm{Kn_r}u_1=&\frac{(a+1)p_0'}{\gamma(a+2)\Delta T_{a+1}^2}\Big(T_0^{a+2}-\frac{\Delta T_{a+2}}{\Delta T_1}T_0+\frac{\Delta T_{a+1}T_{w1}T_{w2}}{\Delta T_1}\Big)\\ &+\mathrm{Kn_r}(f_1T_0^{a+2}+f_2T_0+f_3T_0^{-a}+f_4)\end{aligned} \tag{2.34}$$

$$p=p_0+\mathrm{Kn_r}p_1=p_0+\mathrm{Kn_r}\Big[\frac{C_{IV}}{C_{II}}\Big(\frac{1}{p_0}-1\Big)+\frac{C_{IV}\Big(1-\Pi\Big)}{C_{II}p_0}(x-1)\Big] \tag{2.35}$$

$$\dot m=\frac{C_{II}}{2}(1-\Pi^2)+\mathrm{Kn_r}C_{IV}(1-\Pi) \tag{2.36}$$

where T_0, and p_0 are solutions in the continuum regime with variable transport coefficients (2.7) and (2.9) respectively. Functions of the streamwise coordinates x, f_1, f_2, f_3, f_4, and C_{IV} are constant:

$$
\begin{aligned}
f_1 &= \frac{(a+1)p_1'}{\gamma(a+2)\Delta T_{a+1}^2} + \frac{a\alpha_T \Delta T_{a+0.5+} p_0'}{\gamma(a+2)\Delta T_{a+1}^2 p_0} \\
f_2 &= -\frac{(a+1)\Delta T_{a+2} p_1'}{\gamma(a+2)\Delta T_{a+1}^2 \Delta T_1} + \frac{\alpha_v p_0'}{\gamma \Delta T_{a+1}\Delta T_1 p_0}\Big(\frac{\Delta T_{a+2}\Delta T_{0.5+}}{(a+2)\Delta T_1} - \Delta T_{a+1.5+}\Big) \\
&\quad + \frac{\alpha_T \Delta T_{a+2} p_0'}{\gamma(a+2)\Delta T_{a+1}^2 \Delta T_1 p_0}\Big(\frac{T_{\mathrm{w1}}^{a+0.5} T_{\mathrm{w2}}^{a+0.5}\Delta T_{0.5+}\Delta T_{-a}}{\Delta T_1} - a\Delta T_{a+0.5+}\Big) \\
f_3 &= -\frac{\alpha_T T_{\mathrm{w1}}^{a+0.5} T_{\mathrm{w2}}^{a+0.5}\Delta T_{0.5+}\Delta T_{a+2} p_0'}{\gamma(a+2)\Delta T_1 \Delta T_{a+1}^2 p_0} \\
f_4 &= \frac{T_{\mathrm{w1}} T_{\mathrm{w2}}}{\gamma(a+2)\Delta T_1 \Delta T_{a+1}}\Big((a+1)p_1' + \frac{(a\alpha_T + 2\alpha_v + a\alpha_v)\Delta T_{a+0.5+} p_0'}{p_0} \\
&\quad - \frac{\alpha_T T_{\mathrm{w1}}^{a+0.5} T_{\mathrm{w2}}^{a+0.5}\Delta T_{a+2}\Delta T_{-a-1}\Delta T_{0.5+} p_0'}{\Delta T_1 \Delta T_{a+1} p_0} - \frac{\alpha_v \Delta T_{-0.5+}\Delta T_{a+2} p_0'}{\Delta T_1 p_0}\Big) \\
C_{IV} &= \frac{\alpha_v \Delta T_{a+1}}{(a+1)\Delta T_1}\Big[\frac{(a+1)\Delta T_{0.5+}\Delta T_{a+2}}{\gamma(a+2)\Delta T_1 \Delta T_{a+1}^2}\Big(1 - \frac{(a+1)T_{\mathrm{w1}}^{0.5} T_{\mathrm{w2}}^{0.5}\Delta T_a}{a\Delta T_{a+1}}\Big) \\
&\quad - \frac{a+1}{\gamma \Delta T_{a+1}^2}\Big(\Delta T_{a+1.5+} - \frac{(a+1)T_{\mathrm{w1}} T_{\mathrm{w2}}\Delta T_a \Delta T_{a+0.5+}}{a\Delta T_{a+1}}\Big)\Big] \\
&\quad + \alpha_T\Big[\frac{T_{\mathrm{w1}}^{0.5} T_{\mathrm{w2}}^{0.5}\Delta T_{0.5}}{\gamma \Delta T_{a+1}^2}\Big(\frac{\Delta T_a \Delta T_{a+2}}{a(a+2)\Delta T_1^2} - T_{\mathrm{w1}}^a T_{\mathrm{w2}}^a\Big) + \Delta T_{a+0.5+} C_{II}\Big]
\end{aligned}
$$

The relation between ratios of mass flow rates in the slip (2.36) and continuum (2.10) flow regimes, and pressure ratios Π, for variable transport coefficients can be expressed as:

$$
\frac{\dot m}{\dot m_0} = 1 + \mathrm{Kn_r}\frac{2C_{IV}}{C_{II}(1+\Pi)}. \tag{2.37}
$$

3. Numerical analysis

All four problems that have been previously analyzed have been conducted with commercial CFD code Ansys Fluent. Generally, two main types of solvers are available: pressure-based and density-based. The problems in both continuum and slip flow regimes can be solved with each solver. In the present paper, a density-based solver has been selected. With this solver problems in the continuum and slip flow regimes can be solved by selecting proper boundary conditions. For flows in the slip flow regime, there is partial slip boundary condition for rarefied gases (PSRG)[13]. This boundary condition incorporates the velocity slip and temperature jump, and is applied at the top and bottom walls of the microchannel. It is automatically applied if the flow is in the slip regime, i.e. Knudsen number is between $0.01 < \mathrm{Kn} < 0.2$ [13].

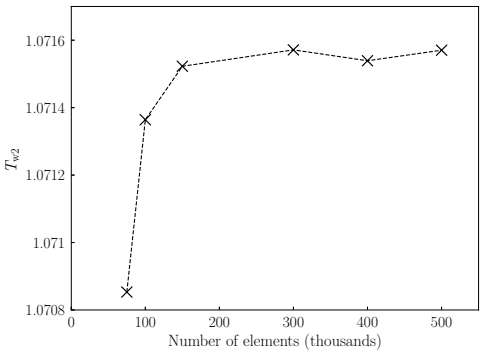

FIGURE 2. Effect of mesh refinement to non-dimensional gas temperature

In this study, argon, a monoatomic gas, has been selected as the working gas. Now the process of configuring software for both continuum and rarefied gas flow regimes, with both constant and variable dynamic viscosity and thermal conductivity is going to be presented. In the case of variable transport coefficients, power law (1.6) has been used. Ansys Fluent has some predefined methods for defining both transport coefficients. The power law is available for dynamic viscosity, while for thermal conductivity it has to be inserted manually as an expression. In the slip flow regime, values of Knudsen numbers are within $\mathrm{Kn} < 0.1$. To ensure that values of reference Knudsen number remain within this domain throughout the entire channel, appropriate values of pressure and temperature have been specified at the outlet cross section.

3.1. Numerical mesh. A numerical mesh has been generated with Ansys Meshing for the flow domain shown in Figure 1, for the channel length of 1000μm and height of 1μm.

The quality of the mesh has been assessed for the most demanding case-the slip flow with variable transport coefficients. The mesh independence has been checked for the reference (outlet) cross section, for values of gas temperature at the upper wall. This is due to the largest temperature jump at this point. Values of nondimensional temperature for different numbers of elements are shown in Figure 2. The mesh independence has been observed for grids with more than 150000 elements. In the present study, all numerical calculations have been conducted with numerical mesh with 300000 elements.

3.2. Boundary conditions and solution methods. For the boundary conditions at the inlet and outlet of the flow domain, pressure inlet and pressure outlet have been selected. Linear temperature distribution has been applied at both inlet and outlet of the flow domain. This has been done to speed up the transition from a specified temperature profile to an actual, numerically obtained profile. This linear distribution is also the exact analytical solution in the continuum regime with constant transport coefficients. For top and bottom walls, no-slip and no-jump

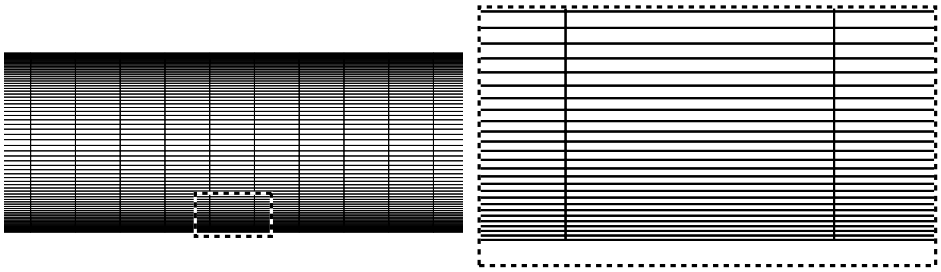

(a) (b)

FIGURE 3. Numerical mesh: a) section of the numerical mesh, b) cropped view, near the bottom wall

boundary conditions have been selected for the continuum regime, and PSRG has been selected for the slip flow regime. The temperature on the bottom wall has been set to 300K, while on the top wall it was set to 366.67K ($\Theta = -0.1$). In this paper, both momentum and thermal accommodation coefficients have been set to unity ($\sigma_v = 1$ and $\sigma_T = 1$).

A density-based solver has implicit and explicit formulations. In the present paper, the implicit formulation has been selected. The flux type has been set to Roe-FDS, under spatial discretization, the gradient has been set to the least squares cell-based, and flow has been set to Third-Order MUSCL [13]. In order to speed up convergence, pseudo time step has been used.

4. Results and discussion

The comparison between analytical and numerical results of pressure, velocity, and temperature distributions, obtained in this paper, is given for four cases that were considered. Both the momentum and thermal accommodation coefficients were set to unity ($\sigma_v = 1$ and $\sigma_T = 1$), which corresponds to diffuse reflection. The ratio of channel height to length was set to $\varepsilon = 0.001$, the reference value of the Prandtl number to $\mathrm{Pr}_\mathrm{r} = 2/3$ (monoatomic gas, as the working fluid [12]), and the temperature difference between the walls was set to $\Theta = -0.1$.

Here, we address the effect of temperature boundary conditions at the inlet cross section. It is important to note that when we refer to the numerical results at $x = 0$, they were, in fact, obtained at the slightly downstream location of $x = 0.05$. The reason for this adjustment is that in the Ansys Fluent temperature boundary condition is required. It has been confirmed the full development of the temperature profile is present at this cross section.

The results in the continuum flow regime with constant transport coefficients are presented in Figures 4 and 5. Figure 4 presents a comparison between analytical and numerical pressure distributions for various pressure ratios at the inlet and outlet cross-sections ($\Pi \in \{2, 3, 5, 10\}$). In Figure 5, the velocity and temperature distribution is depicted, with a chosen pressure ratio of $\Pi = 5$. Overall, excellent agreement in both pressure, velocity and temperature distributions is present.

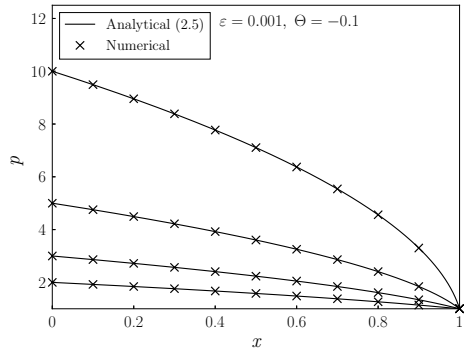

FIGURE 4. Pressure distribution in the continuum flow regime with constant transport coefficients

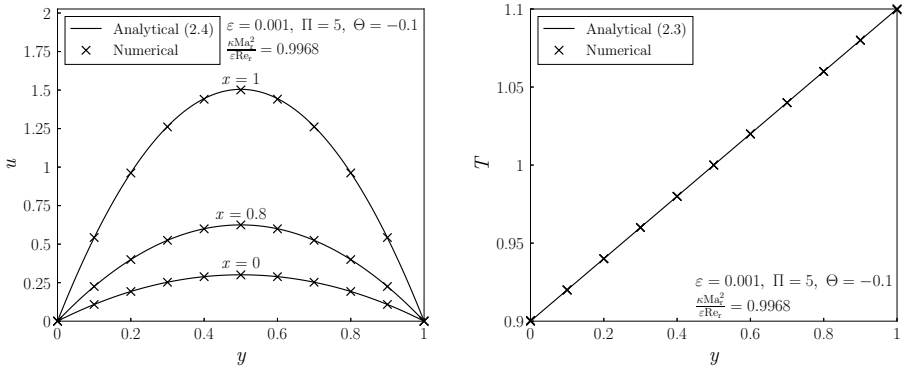

(a) (b)

FIGURE 5. Continuum flow regime with constant transport coefficients: a) velocity and b) temperature distribution

Temperature distribution is linear and remains the same at all cross sections, according to analytical solution (2.3).

The results in the continuum flow regime with variable transport coefficients are presented in Figures 6 and 7. In the power law expression (1.6), as well as in the numerical analysis, viscosity-temperature index a was set to 0.8. In Figure 6 pressure distribution is given for pressure ratios at the inlet and outlet cross sections $\Pi \in \{2, 3, 5, 10\}$, while in figure 7 velocity and temperature distribution are presented for $\Pi = 5$. The temperature distribution remains the same across all cross sections, but is now nonlinear. This nonlinearity arises from the dependence of transport coefficients on temperature (2.7).

In Figures 8–11 we present results in the rarefied gas flow regime, where reference Knudsen number was set to $\mathrm{Kn}_\mathrm{r} = 0.1$. This ensures that flow remains in the slip flow regime.

The results for the rarefied gas flow regime with constant transport coefficients are presented in Figures 8 and 9. In Figure 8 comparison between analytical and numerical results for pressure distribution is given for $\Pi \in \{2, 3, 5, 10\}$. In Figure 9 the velocity and temperature distributions are shown for a pressure ratio of $\Pi = 5$. The results for all pressure ratios exhibit excellent agreement. Temperature distribution is nonlinear, and is different in all cross sections (2.23). In the velocity and temperature distributions, excellent agreement is evident at the inlet and $x = 0.8$ cross-sections, with slight deviation at the outlet cross-section.

The results in the rarefied gas flow regime with variable transport coefficients are presented in Figures 10–11. Again, in the power law expression (1.6), and in the numerical analysis, viscosity-temperature index a was set to 0.8. In Figure 10 pressure distribution is given for $\Pi \in \{2, 3, 5, 10\}$. Velocity and temperature distributions are shown in Figure 10 for $\Pi = 5$. All pressure ratios are in excellent

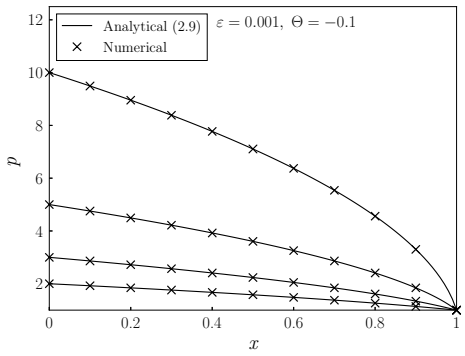

FIGURE 6. Pressure distribution in the continuum flow regime with variable transport coefficients

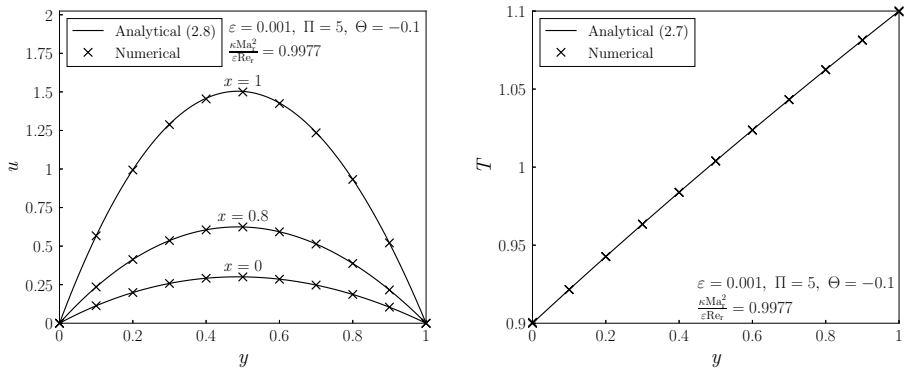

(a) (b)

FIGURE 7. Continuum flow regime with variable transport coefficients: a) velocity and b) temperature distribution

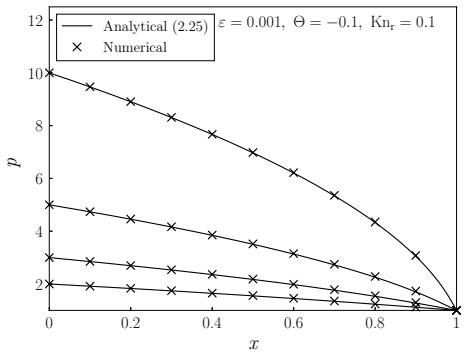

FIGURE 8. Pressure distribution in the rarefied gas flow regime with constant transport coefficients

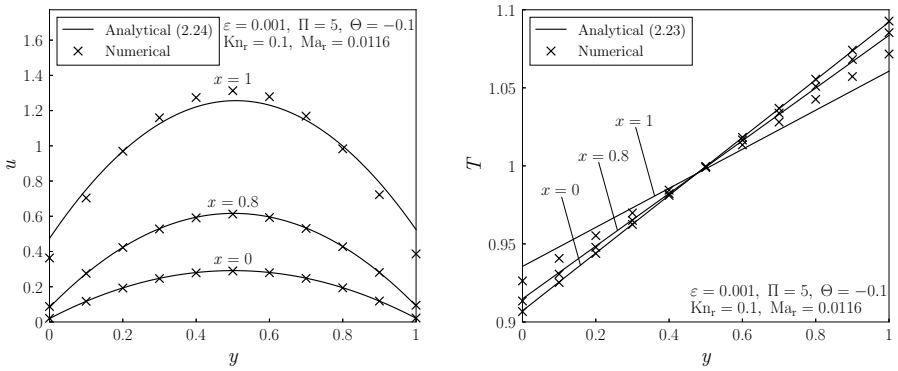

(a) (b)

FIGURE 9. Rarefied gas flow regime with constant transport coefficients: a) velocity and b) temperature distribution

agreement. Again, temperature distribution is nonlinear (2.33). Similarly, a good agreement is observed for the velocity and temperature distributions, with a slight deviation at the outlet cross section.

The largest absolute differences between analytical and numerical solutions for the continuum and rarefied gas flow regimes for velocity, pressure and temperature distributions were calculated according to the following expression:

$$\|\phi_{\mathrm{an}} - \phi_{\mathrm{num}}\|_\infty = \sup_{y\in[0,1]} |\phi_{\mathrm{an}} - \phi_{\mathrm{num}}|$$

where ϕ represents the velocity, pressure and temperature fields. All absolute differences were calculated for pressure ratio $\Pi = 5$. In the continuum flow regime, with and without constant transport coefficients, the largest absolute difference in velocity distribution is 0.004697, in pressure distribution it is 0.000056, while the largest absolute difference in temperature distribution is 0.000627. In the rarefied gas flow regime, with both constant and variable transport coefficients, the largest

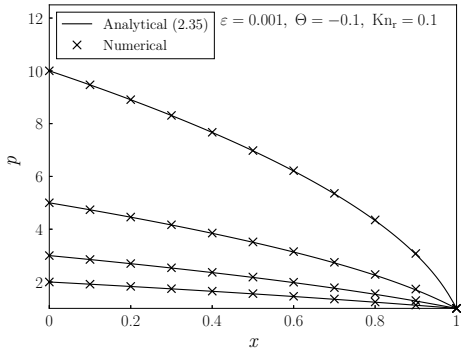

FIGURE 10. Pressure distribution in the rarefied gas flow regime with variable transport coefficients

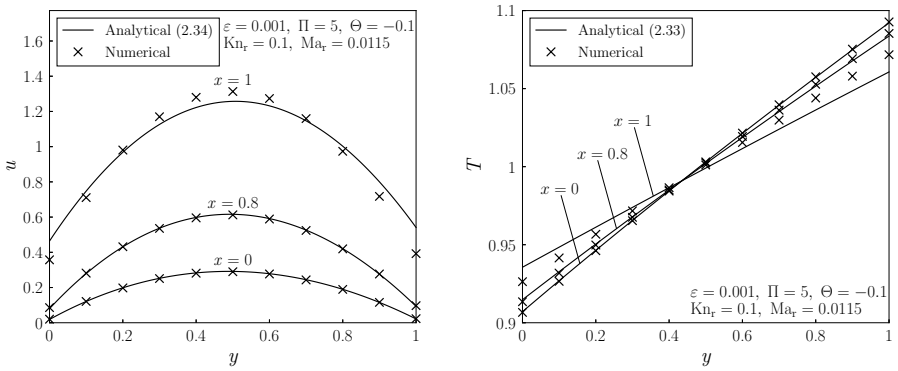

(a) (b)

FIGURE 11. Rarefied gas flow regime with variable transport coefficients: a) velocity and b) temperature distribution

absolute difference in velocity distribution is 0.146788, in pressure distribution it is 0.032965, while the largest absolute difference in temperature distribution is 0.011032.

These discrepancies in the rarefied gas flow regime can be attributed to differences in the analytical system of equations (1.15)–(1.19) where some terms were neglected, and the full system of equations which was applied to the numerical simulation. Also, the approximate approach in the analytical solutions led to the differences in the analytical and numerical results. Finally, the deviation could be reduced by improving the numerical scheme.

The analytically and numerically obtained ratios of mass flow rates in the rarefied and continuum flow regimes for various pressure ratios are provided in Figure 12. Dependence of transport coefficients on temperature was applied, which corresponds to analytical expression (2.37). The influence of rarefaction manifests as an

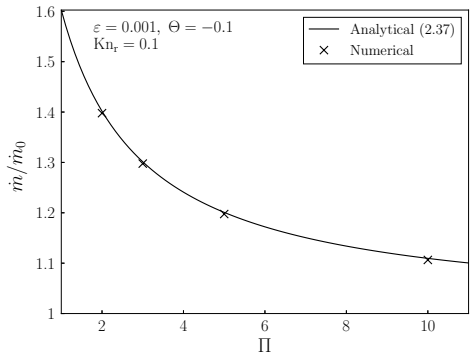

FIGURE 12. Ratio of mass flow rates for different pressure ratios in the rarefied gas flow and continuum flow regimes

excess in mass flow rate, which is more pronounced for smaller pressure ratios. In general, we observe excellent agreement between analytical and numerical solutions for all pressure ratios. Despite slightly larger disagreements are observed in the velocity profile at the outlet cross section for the rarefied gas flow regime between analytical and numerical results, the mass flow rates exhibit excellent agreement, with absolute differences between analytical and numerical results remaining below 0.002666.

5. Conclusions

In this paper, we obtained analytical solutions for nonisothermal compressible problems in the continuum and the rarefied gas flow regimes. The analytical solutions in the continuum regime were exact, while the solutions in the slip flow regime were obtained using the perturbation method. We compared those analytical solutions with numerical results obtained with Ansys Fluent.

It has been shown that for problems in the continuum flow regime, with both constant and variable transport coefficients, there is a perfect matching between analytical and numerical results. In the case of rarefied gas flows, there is also a good agreement for pressure, velocity, and temperature fields between analytical and numerical solutions. A slight difference is present for velocity and temperature profiles at the channel outlet, which is attributed to the differences in the analytical and numerical systems of equations that are being solved, as well as that the analytical solution is an approximate one, and finally due to imperfections in the numerical scheme. Furthermore, the ratios of mass flow rates in the rarefied and continuum flow regimes, across varying ratios of inlet and outlet pressures is analyzed analytically and numerically. A very good consistency is present. Notably, the increase in mass flow rate due to rarefaction is more pronounced for smaller pressure ratios.

In conclusion, Ansys Fluent is a suitable tool for both continuum and slip flow regimes. This CFD code allows future exploration of flow domains where exact analytical solutions are either impossible to obtain or the process of obtaining

them is quite demanding. This also opens up possibilities to explore flows with more complex geometries and boundary conditions.

References

1. M. Gad-El-Hak, *The MEMS Handbook*, CRC Press, Boca Raton, Florida, 2002.
2. A. Beskok, G. Karniadakis, *Microflows and Nanoflows: Fundamentals and Simulation*, Interdiscip. Appl. Math., Springer, 2005.
3. F. Sharipov, *Rarefied gas flow through a long rectangular channel*, J. Vac. Sci. Technol. A **17**(5) (1999), 3062–3066.
4. A. Agrawal, *A Comprehensive review on gas flow in microchannels*, Int. J. Micro Nano Scale Transp. **2**, (2011), 1–40.
5. H. Akhlaghi, E. Roohi, S. Stefanov, *A Comprehensive review on micro-and nano-scale gas flow effects: Slip-jump phenomena, Knudsen paradox, thermally-driven flows, and Knudsen pumps*, Phys. Rep. **997** (2023), 1–60.
6. T. J. Scanlon, E. Roohi, C. White, M. Darbandi, J. M. Reese, *An open source, parallel DSMC code for rarefied gas flows in arbitrary geometries*, Computers & Fluids **39** (2010), 2078–2089.
7. M. Spiga, P. Vocale, *Slip flow in elliptic microducts with constant heat flux*, Adv. Mech. Eng. **4** (2012), 481280.
8. J. Pitakarnnop, R. Wongpithayadisai, S. Phanakulwijit, *Alternative models and numerical simulations of rarefied gas flow in vacuum systems*, Measurement **126** (2018), 417–420.
9. V. Leontidis, J. Chen, L. Baldas, S. Colin, *Numerical Design of a Knudsen Pump with Curved Channels Operating in the Slip Flow Regime*, Heat and Mass Transfer **50** (2014), 1065–1080.
10. W. G. Vincenti, C. H. Kruger, *Introduction to Physical Gas Dynamics*, John Wiley & Sons, New York, 1965.
11. N. Stevanović, *Rarefied Gas Flows in Microchannels*, Faculty of Mechanical Engineering, University of Belgrade, Belgrade, Serbia, 2010.
12. S. Milićev, *Nonisothermal Compressible Gas Flow in Microchannels*, Faculty of Mechanical Engineering, University of Belgrade, Belgrade, Serbia. [To be published]
13. *Ansys Fluent Theory Guide*, Ansys, Inc., Canonsburg, 2023.
14. J. C. Maxwell, *On stresses in rarefied gases arising from inequalities of temperature*, Phil. Trans. R. Soc. London **170** (1879), 231–256.
15. M. Von Smoluchowski, *Ueber Warmeleitung in verdunnten Gasen*, Ann. Phys. Chem. **64** (1898), 101–130.

АНАЛИТИЧКА И НУМЕРИЧКА АНАЛИЗА НЕИЗОТЕРМСКОГ СТИШЉИВОГ СТРУЈАЊА РАЗРЕЂЕНОГ ГАСА ИЗМЕЂУ ПАРАЛЕЛНИХ ПЛОЧА

Резиме. Када су димензије струјног домена мале, као што је случај у микро-електро-механичким системима (MEMC) и нано-електро-механичким системима (НЕМС), ефекти разређености постају значајни. Овде се разматрају струјања гаса у условима континуума и разређености. Добијена су решења за стишљива неизотермска струјања између паралелних плоча различитих температура. Врши се поређење резултата добијених нашим аналитичким приступом и резултата добијених нумерички комерцијалним CFD кодом Ansys Fluent. Анализирана су четири случаја у условима континуума и разређености са константним и променљивим транспортним коефицијентима. Постигнуто веома добро слагање аналитичких и нумеричких резултата како у области континуума, тако и у области струјања гаса са клизањем. То потврђује могућност решавања проблема анализираних у овом раду применом комерцијалног CFD кода Ansys Fluent, као и примену овог кода за истраживање случајева за које нема аналитичког решења.

Faculty of Mechanical Engineering
University of Belgrade
Belgrade
Serbia
petar.vulicevic@protonmail.com

(Received 17.10.2023)
(Revised 26.11.2023)
(Available online 15.12.2023)